Molecular-beam optical Stark spectroscopy of ScO

Jeffrey Shirley, Chris Scurlock, and Timothy Steimle

Citation: The Journal of Chemical Physics **93**, 1568 (1990); doi: 10.1063/1.459135
View online: http://dx.doi.org/10.1063/1.459135
View Table of Contents: http://scitation.aip.org/content/aip/journal/jcp/93/3?ver=pdfcov
Published by the AIP Publishing

Molecular-beam optical Stark spectroscopy of ScO

Jeffrey Shirley, Chris Scurlock, and Timothy Steimle
Department of Chemistry, Arizona State University, Tempe, Arizona 85287-1604

(Received 19 March 1990; accepted 23 April 1990)

The molecular-beam optical Stark spectrum of the $A\,^2\Pi(v=1)$–$X\,^2\Sigma^+(v=0)$ band system of ScO has been recorded and analyzed. The experimentally determined permanent electric dipole moments of the $A\,^2\Pi_{3/2}$, $A\,^2\Pi_{1/2}$, and $X\,^2\Sigma^+$ states are 4.06(3), 4.43(2), and 4.55(8) D, respectively. The determined hyperfine parameters for the $A\,^2\Pi$ state are $a = 135(1)$ MHz, $d = 177(2)$ MHz, and $eQq_0 = -83(12)$ MHz. The spectroscopic parameters are interpreted in terms of plausible models for the electronic nature of the $A\,^2\Pi$ and $X\,^2\Sigma^+$ states and are compared with theoretical values.

I. INTRODUCTION

The diatomic oxides of the $3d$ transition metals are simple chemical systems for which a description of bonding invokes the ideas of oxygen π–electron back donation, $4s$–$3d$ metal hybridization, multiple d orbital bonding, strong σ bond formation between the metal $4s$ and oxygen $2p$ orbital, and substantial charge transfer between the metal and oxygen atom.[1,2] There is a significant spectroscopic data base for this group of transition metal oxides (TMO)[3] which can be used to establish trends in these bonding contributions as a function of atomic number. Magnetic hyperfine (mhf) parameters and the permanent electric dipole moment are physical properties that can be readily related to bonding properties. The magnetic hyperfine interaction is a sensitive probe of the chemically important valence electrons since it is the average of various functions of the unpaired electron coordinates in the region of the nuclei with nonzero spin. Although qualitative insight about bonding is provided from the analysis of spectra exhibiting mhf structure, detailed comparisons with theoretical values have been hindered by inaccuracy of the *ab initio* wave functions in the region of the nuclei. In contrast, the permanent electric dipole moments, which are a sensitive probe of the overall ionic nature of the bond, are routinely predicted on the basis of *ab initio* wave functions and thus do provide an avenue for quantitative comparison between bonding models and experimentation. Dipole moments are also used in the description of many physical phenomena, such as the interaction with electromagnetic radiation.

The limited number (three) of valence electrons and the low atomic number of scandium makes scandium monoxide, ScO, an optimal TMO for experimental and theoretical studies. Here we report on the results of a molecular-beam optical Stark study of the $A\,^2\Pi(v=1)$–$X\,^2\Sigma^+(v=0)$ band system of ScO. An extensive review of the spectroscopy of ScO can be found in the previous publication describing the results of a molecular-beam optical and radio-frequency optical double resonance study.[4] Particularly worth noting is the previous work of Rice and Field,[5] where values of 4.13(21) and 4.25(25) D for the dipole moments of the $A\,^2\Pi_{3/2}$ and $A\,^2\Pi_{1/2}$ states, respectively, were obtained from the analysis of the Stark effect of the Doppler limited optical spectra. Jueng *et al.*[6] predict dipole moments of 4.04 and 2.69 D, while Bauschlicher and Langhoff[7] predict values of 4.17 and 3.22 D for the $A\,^2\Pi$ and $X\,^2\Sigma^+$ states, respectively. Dolg *et al.*[8] predict a value of 3.60 D for the $X\,^2\Sigma^+$. There have been no predictions for mhf parameters.

II. EXPERIMENTAL AND OBSERVATIONS

The experimental apparatus is identical to that used in the dipole measurement of YO.[9] As in the previous beam study of ScO (Ref. 4), a small tantalum crucible containing Sc metal and Sc_2O_3 was heated to approximately 2500 K by electron bombardment. The LIF was detected through an interference filter (10 nm FWHM) centered at 610 nm. The optical transitions could readily be identified from the assignment given by Rice and Field.[5] Due to the inherent weakness of the $A\,^2\Pi(v=1)$–$X\,^2\Sigma^+(v=0)$ band system, because of the small Franck–Condon factor, $\sim$100 mw of laser radiation was used with no indication of laser power braodening at the linewidth obtainable ($\sim$30 MHz FWHM). A polarization rotator was used to orient the electric field of the radiation parallel to that of the dc electric field. The Stark plate separation was calibrated by measuring the Stark spectra of the $A\,^2\Pi$–$X\,^2\Sigma^+$ optical transitions of CaF.[10]

Zero field studies were initially performed in order to analyze the observed magnetic hyperfine structure of the optical spectrum. A zero field energy level diagram for the lowest rotational levels of the $A\,^2\Pi$ and $X\,^2\Sigma^+$ states of ScO, calculated by a method given below, is presented in Fig. 1. The energy level pattern of the low rotational states of the $X\,^2\Sigma^+$ state is best described by a "case $b_{\beta S}$" coupling scheme with $G(=I+S)$ being the approximately good intermediate quantum number. Each ground state rotational level is split into two components ($G = 3,4$) of identical parity separated by the Sc ($I = 7/2$) magnetic hyperfine splitting. These levels are further split into $2G+1$ levels by the spin–rotation interaction and labeled by $F(=N+G)$, the total angular momentum. The energy level pattern of the low rotational levels of the $A\,^2\Pi$ state is that of a near "case $a_{\beta J}$" molecule where the approximately good intermediate quan-

 0021-9606/90/151568-08$03.00

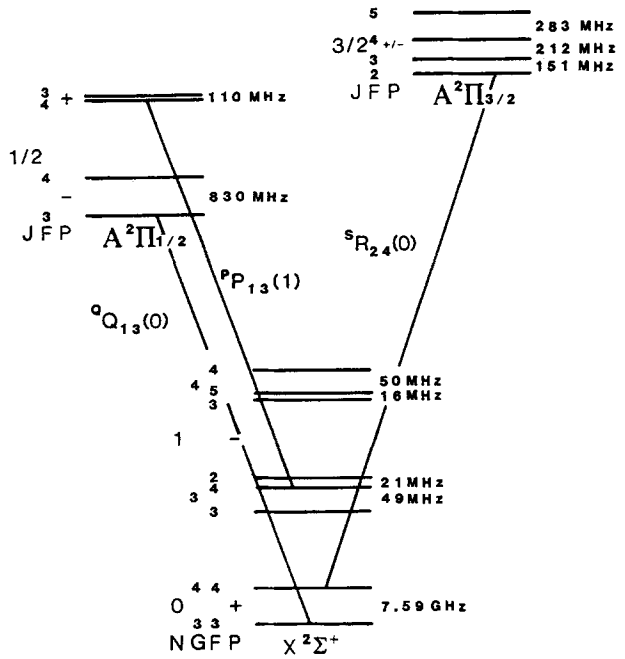

FIG. 1. The zero-field low rotational energy levels of the $A\,^2\Pi(v=1)$ and $X\,^2\Sigma^+(v=0)$ states of ScO, calculated using the ground state parameters of Refs. 4 and 14, and the excited state fine structure parameters estimated from the results of Ref. 14 and the determined hyperfine parameters of this work. The optical transitions studied in the Stark experiments are indicated. The energy levels are not drawn to scale.

tum number is J. Each rotational state consists of a pair of levels, labeled by J, which have opposite parity and are split by the Λ-doubling. Each Λ-doublet is split into hyperfine components labeled by $F(=J+I)$.

The energy levels of Fig. 1 are not drawn to scale. The splitting between the $G=3$ and $G=4$ components of the $N=0$ level of the $X\,^2\Sigma^+$ state is ~7.6 GHz and stays fairly constant as a function of N, whereas for example the splitting between the $N=1$; $G=3$; $F=3$ and the $N=1$; $G=3$; $F=4$ levels is 49 MHz. The Λ-doubling in the $A\,^2\Pi_{1/2}$ $J=0.5$ level is ~2.0 GHz while the splitting between the $F=3$ and $F=4$ hyperfine levels of the $p=''-''$ component of that Λ-doublet is ~830 MHz. The Λ-doubling in the $J=1.5$ level of the $A\,^2\Pi_{3/2}$ state is <1 MHz, while the splitting between the $F=2$ and $F=3$ hyperfine levels is 151 MHz.

The branch labeling scheme is a modified version of the more commonly occurring $^2\Pi$ (case a)–$^2\Sigma$(case $b_{\beta J}$) band system scheme, where the second subscript of the branch designation, the $X\,^2\Sigma^+$ F_i label ($i=1$ or 2 for $J=N+S$ or $N-S$), is replaced with the $G(=I+S)$ value. The eight branch features of the $^2\Pi_{1/2}$ (case a)–$^2\Sigma$(case $b_{\beta S}$) subband are designated ${}^{O}P_{1G}$, ${}^{P}P_{1G}+{}^{P}Q_{1G}$, ${}^{Q}Q_{1G}+{}^{Q}R_{1G}$, and ${}^{R}R_{1G}$ while the eight branch features of the $^2\Pi_{3/2}$(case a)–$^2\Sigma$(case $b_{\beta S}$) subband are designated ${}^{P}P_{2G}$, ${}^{Q}P_{2G}+{}^{Q}Q_{2G}$, ${}^{R}Q_{2G}+{}^{R}R_{2G}$, and ${}^{S}R_{2G}$ with $G=3$ and 4 for ScO. In all that follows we have used the abbreviation ${}^{Q}Q={}^{Q}Q+{}^{Q}R$, ${}^{P}P={}^{P}P+{}^{P}Q$, and ${}^{R}Q={}^{R}Q+{}^{R}R$. Eight optical transitions were studied in order to determine the excited state hyperfine interaction. The zero field spectra of the ${}^{S}R_{24}(0)$ and ${}^{P}P_{13}(14)$ branch features are presented in Fig. 2. In these two examples, the splittings are due primarily to the excited state hyperfine effects (see Fig. 1). The measured hyperfine splittings in the eight branch features are given in Table I.

The ${}^{Q}Q_{13}(0)$, ${}^{P}P_{13}(1)$, and ${}^{S}R_{24}(0)$ branch features were selected for the optical Stark measurements (see Fig. 1). The ${}^{S}R_{24}(0)$ optical Stark spectrum at two field strengths is presented in Fig. 3. Because of the near degeneracy of the Λ-doublets of the $A\,^2\Pi_{3/2}$ state, the spectral pattern is a strong function of dc field strength. The large mhf structure in the excited state associated with this transition (see Figs. 1 and 2) is responsible for the complex Stark pattern. The splittings were measured directly using the transmission peaks of a temperature controlled etalon. Note that at high dc fields, where M_J becomes the approximately good quantum number, the pattern would become a set of four $(=2J+1)$ nearly equally spaced groups of transitions as observed by Rice and Field.[5]

The optical Stark spectra of the ${}^{Q}Q_{13}(0)$ and ${}^{P}P_{13}(1)$ branch features are presented in Fig. 4. The upper states of these two branch features are the two opposite parity Λ-doublets of the $A\,^2\Pi$, $J=0.5$ level. The Λ-doubling in the $J=0.5$ level is ~2 GHz and thus the energy levels exhibit a

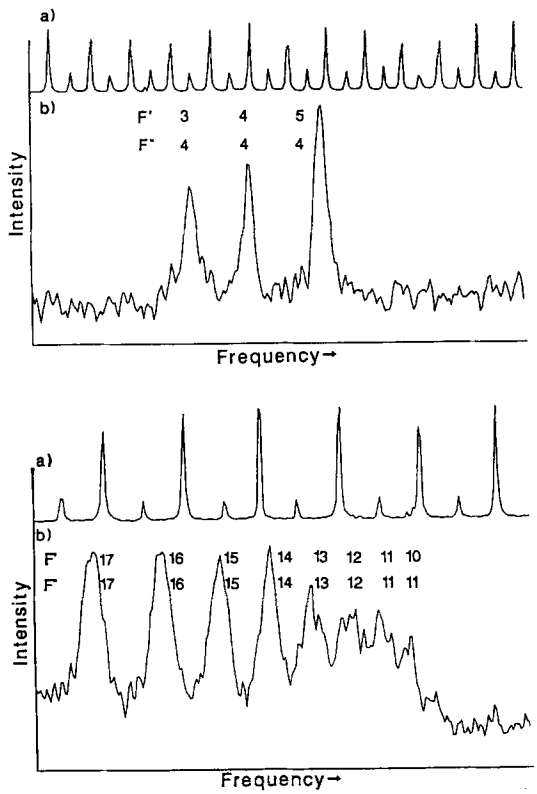

FIG. 2. The zero-field molecular-beam LIF spectrum of the ${}^{S}R_{24}(0)$ (top) and ${}^{P}P_{13}(14)$ (bottom) branch features of the $A\,^2\Pi(v=1)$–$X\,^2\Sigma^+(v=0)$ band system and the transmission of a 77.4 MHz F.S.R. etalon. The splitting is due primarily to hyperfine interactions in the $A\,^2\Pi(v'=1)$ state.

TABLE I. Observed and calculated zero-field hyperfine splittings.

Rotational[a] transition	F' upper	F' lower	F'' upper	F'' lower	Splitting (MHz) obs	Splitting (MHz) calc	obs − calc (MHz)
$^{P}P_{13}(2)$	5	4	5	5	156	158	− 2
	4	3	5	4	109	113	− 4
$^{P}P_{13}(3)$	6	5	6	6	163	148	15
	5	4	6	5	115	114	1
	4	3	5	4	87	86	1
	3	2	4	3	55	61	− 6
	2	1	3	2	34	39	− 5
$^{P}P_{13}(14)$	16	17	16	17	103	111	− 8
	15	16	15	16	103	101	2
	14	15	14	15	96	91	5
	13	14	13	14	86	82	4
	12	13	12	13	70	74	− 4
	11	12	11	12	64	66	− 2
	10	11	11	11	47	58	− 9
$^{S}R_{24}(0)$	5	4	4	4	281	283	− 2
	4	3	4	4	229	212	17
$^{R}Q_{23}(1)$	5	4	4	4	276	283	− 7
	4	3	4	4	220	212	8
	3	2	4	3	149	151	− 2
$^{S}R_{24}(1)$	6	5	5	4	144	136	8
	5	4	4	4	121	116	5
	4	3	4	3	90	94	− 4
$^{S}R_{23}(1)$	5	4	4	3	107	116	− 9
$^{R}Q_{24}(1)$	5	4	4	3	276	283	− 7
	4	3	3	3	211	212	− 1
	3	2	3	3	148	151	− 3

[a] The abbreviation $^{Q}Q = {}^{Q}Q + {}^{Q}R$, $^{P}P = {}^{P}P + {}^{P}Q$, and $^{R}Q = {}^{R}Q + {}^{R}R$ for the branch designation has been used throughout the manuscript.

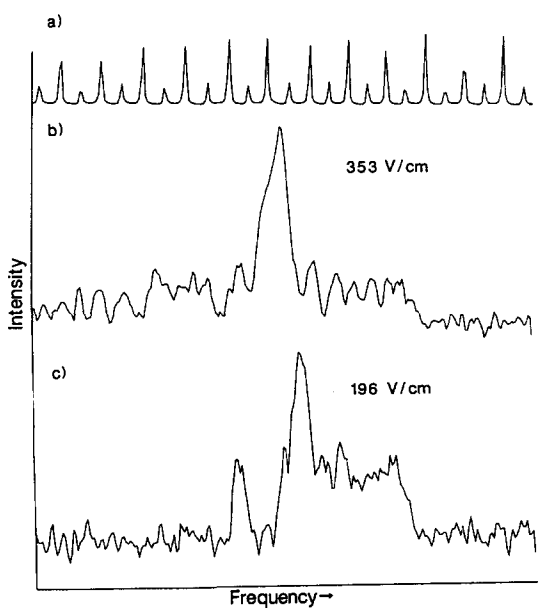

FIG. 3. The transmission of the 77.4 F.S.R. etalon (a) and the optical Stark spectrum of the $^{S}R_{24}(0)$ $A\,^{2}\Pi(v=1)$–$X\,^{2}\Sigma^{+}(v=0)$ branch feature at two field strengths at (b) 340 V/cm and (c) 196 V/cm. The numerous weak features are reproducible and agree with the energy level pattern of Fig. 7.

pseudo-first-order Stark effect. The upper levels of the $^{P}P_{13}(1)$ branch feature shift rapidly to higher energy and accordingly the transition moves to higher frequency when the dc field is applied (see Fig. 4). The opposite situation arises for the $^{Q}Q_{13}(0)$ feature. For these measurements, the shifts were obtained by scanning the laser frequency across the optical feature at a fixed field strength, then momentarily stopping the scan and either turning on or off the dc field and then continuing the scan. At the higher field strengths the second-order Stark effect of the $X\,^{2}\Sigma^{+}$ levels influence the optical spectra. The measured shifts and splittings, which were used as input into a least-squares-fitting procedure, are given in Table II.

III. ANALYSIS

The effective Hamiltonian for the hyperfine interaction and effects of a dc field are given by[11–13]

$$\hat{H} = \hat{H}_{\text{mhfs}} + \hat{H}_{\text{el.q.}} + \hat{H}_{\text{Stark}}, \tag{1}$$

where

$$\hat{H}_{\text{mhfs}} = a\hat{I}_z\hat{L}_z + b_F\hat{\mathbf{I}}\cdot\hat{S} + c/3(3\hat{I}_z\hat{S}_z - \hat{\mathbf{I}}\cdot\hat{S}) - d/2(e^{2i\phi}\hat{I}_-\hat{S}_- + e^{-2i\phi}\hat{I}_+\hat{S}_+), \tag{2}$$

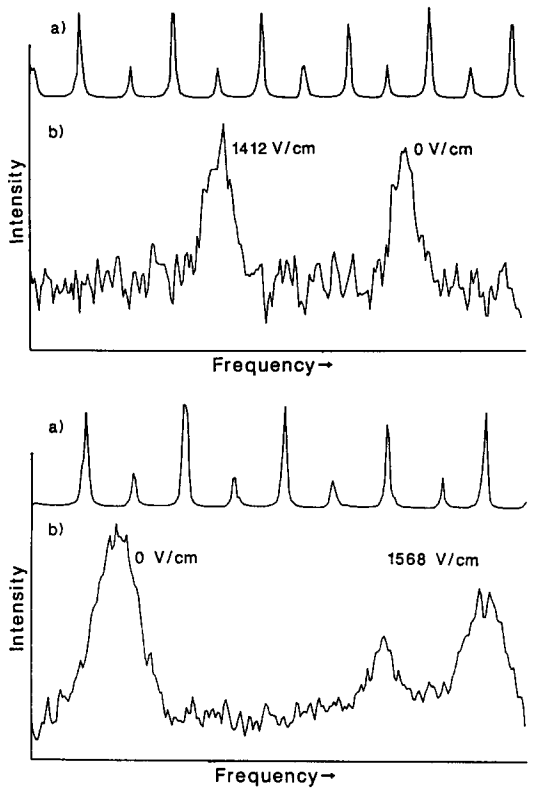

FIG. 4. A portion of the Stark spectrum (a) of the $^{Q}Q_{13}(0)$ branch feature (top) and the $^{P}P_{13}(1)$ branch feature (bottom) of the $A\,^2\Pi(v=1)$–$X\,^2\Sigma^+(v=0)$ band system along with the transmission of a 77.4 MHz F.S.R. etalon. The spectra were recorded by turning on/off the field in the middle of the scan.

$$\hat{H}_{\text{el.q.}} = T^2(\nabla\hat{E})\cdot T^2(\hat{Q}), \tag{3}$$

$$\hat{H}_{\text{Stark}} = -\sum_{pq}(-1)^p T^1_p(\hat{E}) D^{1\,*}_{-pq}(\omega) T^1_q(\hat{\mu}). \tag{4}$$

In Eq. (2), a, b, c, and d are the strengths of the orbital, Fermi contact, dipolar, and Λ-doubling type magnetic hyperfine interactions. The electric quadrupole contribution has been written as the product of the spherical tensor of the electric field gradient, $T^2(\nabla\hat{E})$, with the spherical tensor components of the nuclear quadrupole moment, $T^2(\hat{Q})$. In general, there are five quadrupole parameters associated with the expectation values of the five components of $T^2(\nabla\hat{E})$, but within a $^2\Pi$ state only two have nonzero mean values and are defined as

$$eQq_0 \equiv eQ\langle\Lambda = \pm 1|2T^2_0(\nabla\hat{E})|\Lambda = \pm 1\rangle \tag{5}$$

and

$$eQq_2 \equiv eQ\langle\Lambda = \pm 1|2\sqrt{6}T^2_{\pm 2}(\nabla\hat{E})|\Lambda = \mp 1\rangle. \tag{6}$$

In Eq. (4), $T^1_p(\hat{E})$ and $T^1_q(\hat{\mu})$ are the spherical tensor operators for the static electric field and the dipole moment, respectively. The rotation matrix $D^{1\,*}_{-pq}(\omega)$ relates the molecule and space fixed components of $\hat{\mu}$. In the present experiment the electric field vector of the radiation and the static field were parallel and defined the space fixed Z direction. Accordingly, the matrix representation is block diagonal in M_F and is of infinite dimension.

In the analysis of the zero-field optical spectra a program was written that sets up the complete Hamiltonian representation, performs the diagonalization, and takes the appropriate combinations of eigenvalues to predict splittings in the optical spectra. The calculated splittings as a function of adjustable spectroscopic parameters together with the observed splittings were then used as input to a standard nonlinear least-squares-fitting program. The dimension of the representations were $16(=(2I+1)(2S+1))$ and $32(=2(2S+1)(2I+1))$ for the $X\,^2\Sigma^+$ and $A\,^2\Pi$ states, respectively, in a case $a_{\beta J}$ basis set. All of the $X\,^2\Sigma^+$ state parameters and the rotational and fine parameters of the $A\,^2\Pi$ state were held fixed to the previously determined values.[4,14] The electric quadrupole and magnetic hyperfine parameters of the $A\,^2\Pi$ state were optimized in the least-squares procedure. The data were not extensive enough to determine all six parameters that appear in Eqs. (2) and (3), with the best fit occurring when the parameters a, d, and eQq_0 were used. The determined parameters, associated error estimates, and correlation matrix are given in Table III.

The splittings in the $^{P}P_{13}(2)$, $^{P}P_{13}(3)$, and $^{P}P_{13}(14)$ branch features are particularly sensitive to the value of d because they involve the $A\,^2\Pi_{1/2}$ subband and thus d is well determined. It is expected that b_F will be negligible because to a first approximation the wave function associated with the $A\,^2\Pi$ state has zero spin density at the nucleus. The eQq_2 term of the effective Hamiltonian operator has only off-diagonal elements in a case $a_{\beta J}$ representation and thus because the low rotational levels of the $A\,^2\Pi$ state are nearly those of this limiting coupling scheme, the data are not sensitive to this parameter. It was determined that the dipolar parameter c produce a slightly worse fit than the a parameter. If c is used instead of a, the fitted parameters are (in MHz) $c=399(11)$, $d=81(7)$, and $eQq_0=62(40)$ with an rms $=21$.

The analysis of the Stark spectra was performed in a similar fashion. The Hamiltonian representation is block diagonal in M_F and of infinite dimension, but for practical purposes was truncated at a finite size. The dimension of the $X\,^2\Sigma^+$ state was 64, being composed of all the basis vectors for the $F=2$, 3, 4, and 5 levels. The largest F value in the $A\,^2\Pi$ state associated with the Stark measurement is 5 and ideally a 128×128 matrix composed of the nonparity basis set for the $F=2$, 3, 4, and 5 should have been used. It was impractical to diagonalize this size of matrix to the required accuracy on the microcomputer. Therefore, the matrix was divided into two 64×64 blocks by ignoring the elements that occur between the $^2\Pi_{1/2}$ and $^2\Pi_{3/2}$ blocks. This procedure introduces no error at the accuracy of the measurements of the Stark splittings because the molecule is so near the "case a" limit in the lowest rotational states.

The determination of the permanent electric dipole moments was performed in an iterative fashion. Initially the $A\,^2\Pi$ state values were held fixed to those determined by Rice and Field[5] and the predicted optical Stark spectra were calculated for various values of $\mu(X\,^2\Sigma^+)$. The quantum number assignment of the optical Stark spectrum could be readily assigned by this approach. In the final analysis all of

TABLE II. Observed and calculated Stark shifts/splittings.

Rotational transition	Applied field (V/cm)	Shifts/splitting (MHz)[a] obs	Shifts/splitting (MHz)[a] calc	obs − calc (MHz)
$^{Q}Q_{13}(0)$	1412	− 75	− 71	− 4
	784	− 111	− 108	− 3
	971	− 152	− 153	1
	1098	− 197	− 200	3
	1255	− 257	− 254	− 3
	1412	− 332	− 310	− 22
	1569	− 382	− 371	− 11
$^{P}P_{13}(1)$	784	113	117	− 4
		173	175	− 2
	941	153	169	− 16
		231	237	− 6
	1098	216	225	− 9
		313	307	6
	1755	279	292	− 13
		383	387	− 4
	1412	345	258	− 13
		480	473	7
	1569	408	422	− 14
		563	560	3
$^{S}R_{24}(0)$	78	133	139	− 6
		190	192	− 2
	118	269	288	− 19
	235	144	151	− 7
		284	276	8
		135	122	13
		70	62	8
	275	336	333	3
		143	140	3
		74	73	1
	314	149	136	− 4
		78	82	13
	353	121	112	9
		190	201	− 11
		118	112	6
		137	136	1
		138	137	1
		90	89	1
	392	118	110	8
		238	232	6
		113	101	12
		182	176	6
		154	144	10
		95	94	1

[a] These are measured shifts and splittings between prominent features in the spectra, which are generally composed of many transitions. See Figs. 5, 6, and 7.

the observed Stark shifts or splittings were used in a least-squares-fitting procedure with $\mu(A\,^2\Pi_{1/2})$, $\mu(A\,^2\Pi_{3/2})$, and $\mu(X\,^2\Sigma^+)$ being the adjustable parameters. The results of the least-squares fit are given in Table III. Note that although the values are extracted from an analysis of optical spectra, the correlation of the three dipole moments is not significant. The previous experimental results for the $A\,^2\Pi$ state and the theoretical values are also given in Table III for comparison. The Stark shifts of the energy levels associated with $^{Q}Q_{13}(0)$, $^{P}P_{13}(1)$, and $^{S}R_{24}(0)$ branch features are illustrated in Figs. 5, 6, and 7, respectively. The ρ-doubling and Λ-doubling are not drawn to scale (see above).

IV. DISCUSSION

The low rotational features of the $A\,^2\Pi$–$X\,^2\Sigma^+$ band system of ScO are complicated because of the strong rotational dependence of the magnetic hyperfine, electric quadrupole, and spin–rotation interactions. The standard effective Hamiltonian operator sufficiently describes this complex energy level pattern and the resulting interaction parameters should contain valuable information about the properties of the electronic wave function. The hyperfine parameters are defined as

$$a/\mathrm{MHz} = 10^{-6}(4\pi h)^{-1}2\mu_B g_N \mu_N \mu_0 \langle r^{-3}\rangle, \qquad (7)$$

TABLE III. Hyperfine parameters and dipole moments for ScO.

Hyperfine parameters (MHz)						
a	135(1)[a]					
d	177(2)					
eQq_0	− 83(12)					
rms	6.9 MHz					

Correlation matrix

a	1.00	0.19	0.08
d		1.00	0.16
eQq_0			1.00

Dipole moments (D)

	Experimental		Theory[c]		
	This work	Ref. 5[b]	Ref. 6	Ref. 7	Ref. 8
$\mu(A\,^2\Pi_{1/2})$	4.43(2)	4.25(25)	4.04	3.70	...
$\mu(A\,^2\Pi_{3/2})$	4.06(3)	4.13(21)			...
$\mu(X\,^2\Sigma^+)$	4.55(8)	...	2.96	3.22	3.60
rms 8.7 MHz					

Correlation matrix

$\mu(A\,^2\Pi_{1/2})$	1.00	0.00	0.68
$\mu(A\,^2\Pi_{3/2})$		1.00	0.00
$\mu(X\,^2\Sigma^+)$			1.00

[a] The numbers in parentheses represent a 2σ error estimate.
[b] Experimental determination.
[c] There were no spin orbit effects considered thus only one value is predicted for the $A\,^2\Pi$ state.

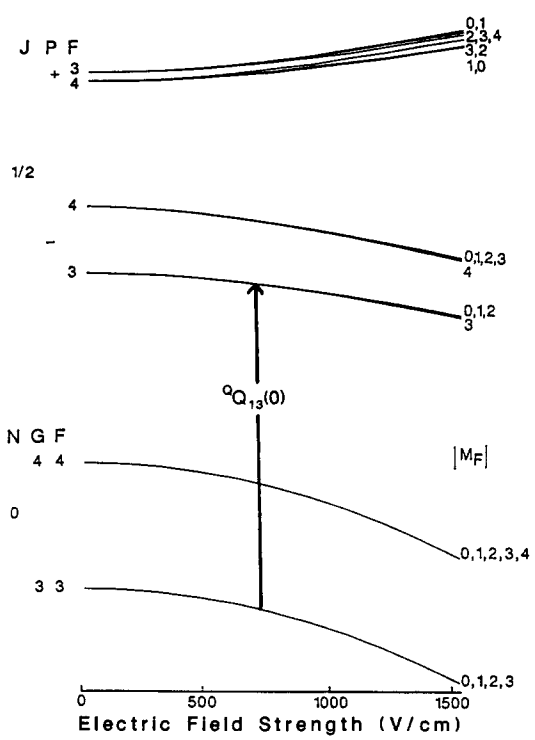

FIG. 5. The energy level pattern as a function of field strength for the levels associated with the $^QQ_{13}(0)$ branch feature.

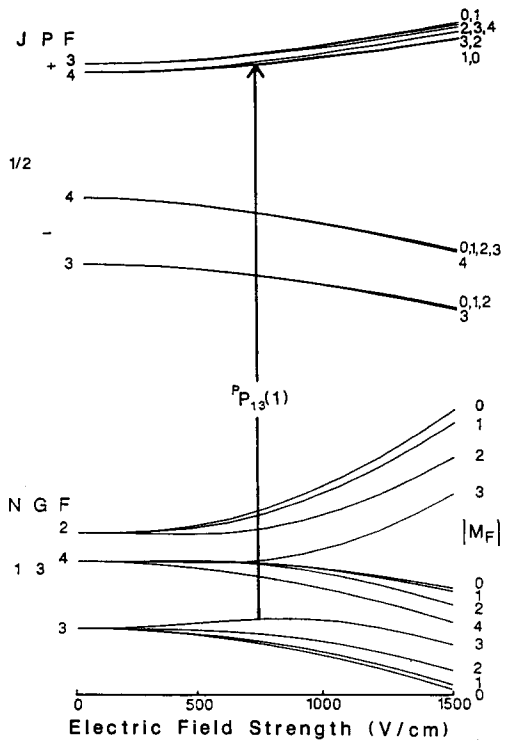

FIG. 6. The energy level pattern as a function of field strength for the levels associated with the $^PP_{13}(1)$ branch feature.

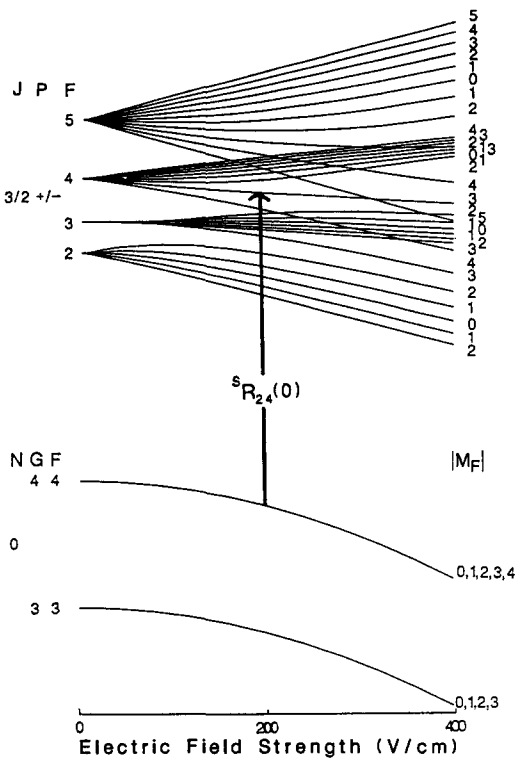

FIG. 7. The energy level pattern as a function of field strength for the levels associated with the $^sR_{24}(0)$ branch feature.

$$d/\text{MHz} = 10^{-6}(8\pi h)^{-1}3g_i\mu_B g_N\mu_N\mu_0\langle\sin^2\theta/r^3\rangle, \quad (8)$$

$$eQq_0/\text{MHz} = 10^{-6}h^{-1}e^2Q\left\langle\sum_i(3\cos^2\theta_i - 1)/r^3\right\rangle, \quad (9)$$

where $\mu_B, \mu_N, g_N, g_i, \mu_0$, and e are the Bohr and nuclear magnetons, nuclear and electron g factors, permeability of free space, and the charge of the electron, respectively. The spherical polar coordinates of the electron are θ and r. In writing Eqs. (7) and (8), it has been assumed that there is a single unpaired valence electron responsible for the magnetic hyperfine structure. The summation in the electric quadrupole parameter is over all the charged particles.

The expectation values of Eqs. (7)–(8) are over the electronic wave function and ideally it would be desirable to have these quantities from the various proposed theoretical models[6–8] in order to make a comparison with the experiment. Even though these numbers are not readily available, it is possible to make a qualitative comparison of the zero-field experimental results with the theoretical predictions based upon knowledge of the atomic orbitals. The $A\,^2\Pi$ state arises from a promotion of the electron in the $4s$ $4p$ hybrid orbital centered on the Sc nuclei in the $X\,^2\Sigma^+$ into a combination of the $3d\pi$ and $4p\pi$ Sc orbitals. The dominant configuration is

$$(\text{core})3\pi^4 7\sigma^2 4\pi \rightarrow {}^2\Pi, \quad (10a)$$

where

$$3\pi \sim 3d\pi(\text{Sc}) + 2p\pi(0), \quad (10b)$$

$$7\sigma \sim 3d\sigma(\text{Sc}) + 2p\sigma(0), \quad (10c)$$

$$4\pi \sim 3d\pi(\text{Sc}) + 4p\pi(\text{Sc}). \quad (10d)$$

According to the results of theoretical models[6–8] the major contribution to the 4π orbital is from the Sc ($3d\pi$) component and for this qualitative comparison it will be assumed to be a pure Sc($3d\pi$) atomic orbital. The angular expectation values that appear in Eqs. (7)–(9) for a $3d\pi$ orbital are $\langle\sin^2\theta\rangle = 4/7$ and $\langle 3\cos^2\theta - 1\rangle = 2/7$ while the radial expectation value can be taken from the atomic beam measurement[15] to be $\langle r^{-3}\rangle = 0.911a_0^{-3}$. Therefore, if the electronic wave function for the $A\,^2\Pi$ state can be adequately described by the single configuration of Eq. (10) and the 4π orbital is assumed to be a pure $3d\pi$ orbital centered upon Sc the predicted values for the magnetic hyperfine parameters are $a = 124$ MHz and $d = 93$ MHz. The agreement with the determined values is fairly good considering this simple model. It is expected that the simple model would more accurately predict "a" because there is no angular dependence for this parameter.

The two contributions to the electric quadrupole parameter are from the field gradient associated with the unpaired electron $(eQq_0)_u$ and the ionic character of the filled bonding orbitals $(eQq_0)_{ib}$,

$$eQq_0 \approx (eQq_0)_u + (eQq_0)_{ib}. \quad (11)$$

The $(eQq_0)_u$ contribution is readily calculated to be -16 MHz using the assumed nature of the single unpaired valence electron and the quadrupole moment of Sc.[16] A screening factor of 0.30 (Ref. 17) and a fractional charge of 0.5 was used in this determination. The majority of the remaining contribution (-67 MHz) to eQq_0 should come from the filled 3π and 7σ molecular orbitals, i.e., $(eQq_0)_{ib}$. If the pair of electrons in the ionic 7σ orbital is solely responsible for $(eQq_0)_{ib}$, then it would be expected that

$$(eQq_0)_{ib} = -67\ \text{MHz} \approx 2\cdot C_1^2 eQq_{320}(1 + c^+\epsilon), \quad (12)$$

where C_1 is the coefficient of the $3d\sigma$ orbital of the 7σ molecular orbital, $eQq_{320}(= -54$ MHz) is the quadrupole coupling of an electron in a $3d$ atomic orbital centered on Sc, c^+ is the fractional positive charge on the Sc (~ 0.5), and ϵ is screening constant[17] (~ 0.30). Substitution of these values into Eq. (15) predicts that $C_1^2 = 0.54$, which is consistent with theory. Thus, the determined value of -83 MHz for eQq_0 is reasonable, and should serve as a critical test of future *ab initio* wave functions.

The dipole moment is a much more sensitive measure of the overall charge distribution in a molecule than are most of the other spectroscopic constants. The value $\mu(X\,^2\Sigma^+)$ is substantially larger than all of the recently published *ab initio* values,[6–8] which is somewhat surprising considering the simplicity of the molecule. Although not published in the recent report on the all electron calculation,[7] it is expected that at the SCF level the predicted dipole moment would be ~ 7 D, similar to that of a point charge model. It is the tendency for the coupled pair functional (CPF) treatment of the configuration interaction to over compensate by mixing in too much covalent character[18] and therefore expected that the value of Ref. 7 will be too low. It is also expected that if the calculation were repeated using the recent approach taken in the determination of μ for CrO (Ref. 18) better agreement would be achieved.

As in the previous measurement,[5] $\mu(^2\Pi_{1/2}) > \mu(^2\Pi_{3/2})$ in magnitude. This is opposite from what was found in YO,[9] where relative magnitudes could be explained by spin–orbit mixing with the $A\,'^2\Delta$ state. It is difficult to derive a simple explanation for the trend in ScO without more details of the electronic states.

V. CONCLUSION

The molecular-beam LIF spectrum of the $A\,^2\Pi(v=1)$–$X\,^2\Sigma^+(v=0)$ band system in both the absence and presence of a static dc electric field has been recorded and analyzed. The determined hyperfine structure parameters for the $A\,^2\Pi$ state could be qualitatively explained in terms of a simple molecular orbital description of this state. A quantitative intepretation would be facilitated by further *ab initio* studies. The determined excited state dipole moments are consistent with the less accurate previously determined values.[5] The dipole moment for the ground state is substantially larger than predictions.

ACKNOWLEDGMENTS

This work was supported by a grant from the National Science Foundation (CHE 8713927). We would like to thank Drs. Richard Suenram (NIST), William Childs (Argonne National Laboratory), and John M. Brown for their helpful comments.

[1]S. R. Langhoff and C. W. Bauschlicher, Jr., Ann. Rev. Phys. Chem. **39**, 181 (1988).
[2]C. W. Bauschlicher, Jr., S. P. Walch, and S. R. Langhoff, *Quantum Chemistry: The Challenge of Transition Metals and Coordination Chemistry*, edited by A. Veillard, NATO ASI Series, Ser. C (Reidel, Dordecht, 1986).
[3]A. J. Merer, Ann Rev. Phys. Chem. **40**, 407 (1989).
[4]W. J. Childs and T. C. Steimle, J. Chem. Phys. **88**, 6168 (1988).
[5]S. F. Rice and R. W. Field, J. Mol. Spectrosc. **119**, 331 (1986).
[6]G. H. Jeung and J. Koutecký, J. Chem. Phys. **88**, 3747 (1988).
[7]C. W. Bauschlicher, Jr. and S. R. Langhoff, J. Chem. Phys. **85**, 5936 (1986).
[8]M. Dolg, U. Wedig, H. Stoll, and H. Pruess, J. Chem. Phys. **86**, 2123 (1987).
[9]T. C. Steimle and J. E. Shirley, J. Chem. Phys. **92**, 3292 (1990).
[10]W. E. Ernst and J. Kandler, Phys. Rev. A **39**, 1575 (1989).
[11]J. M. Brown, I. Kopp, C. Malmberg, and B. Rydh, Physica Scr. **17**, 55 (1978).
[12]C. R. Byfleet, A. Carrington, and D. K. Russell, Mol. Phys. **20**, 271 (1971).
[13]C. M. Western, P. R. R. Langridge-Smith, B. J. Howard, and S. E. Novick, Mol. Phys. **44**, 145 (1981).
[14]R. Stringat, C. Athénour, and J. L. Féménias, Can. J. Phys. **50**, 395 (1972).
[15]W. Ertmer and B. Hofer, Z. Physik A **276**, 9 (1976).
[16]G. Fricke, H. Koppfermann, S. Penselin, and K. Schlömann, Z. Physik **156**, 416 (1959).
[17]W. Gordy and R. Cook, *Microwave Molecular Structure* (Interscience, New York, 1970).
[18]T. C. Steimle, D. F. Nachman, J. E. Shirley, C. W. Bauschlicher, and S. R. Langhoff, J. Chem. Phys. **91**, 2049 (1989).